Title

All-Atom Simulations Uncover Structural and Dynamical Properties of STING Proteins in the Membrane System

Journal

Journal of Chemical Information and Modeling, 62(18)

ISSN

1549-9596

Authors

Payne, Rachel T

Crivelli, Silvia

Watanabe, Masakatsu

Publication Date

2022-09-26

DOI

10.1021/acs.jcim.2c00595

All-Atom Simulations Uncover Structural and Dynamical Properties of STING Proteins in the Membrane System

Rachel T. Payne[1†], Silvia Crivelli[2], and Masakatsu Watanabe[3*]

[1]Boston University, Boston, MA 02215, United States

[2]Lawrence Berkeley National Laboratory, Berkeley, CA 94720, United States

[3]Department of Chemistry, Fort Hays State University, Hays, KS 67601, United States

Present Address:

[†]R.T.P.: Computational Health Informatics Program, Boston Children's Hospital, Boston, MA 02115, United States

*To whom correspondence may be addressed. Email: m_watanabe@fhsu.edu

Abstract

Recent studies have shown that the stimulator of interferon gene (STING) protein plays a central role in the immune system by facilitating the production of Type I interferons in cells. The STING signaling pathway is also a prominent activator of cancer-killing T cells that initiates a powerful adaptive immune response. Since biomolecular signaling pathways are complicated and not easily identified through traditional experiments, molecular dynamics (MD) has often been used to study biological pathways' structural and dynamical responses. Here, we carried out MD simulations for full-length chicken and human STING (chSTING and hSTING) proteins. Specifically, we investigated ligand-bound closed and ligand-unbound open forms of STING in the membrane system by comparing conformational and dynamical differences among them. Our research provides clues for understanding the mechanism of the STING signaling pathway by uncovering detailed insights for the examined systems: the residues from each chain in the binding pocket are 1

strongly correlated to one another in the open STING structure compared with those in the closed STING structure. Ligand-bound closed STING displays ~174° rotation of the ligand-binding domain (LBD) relative to the open STING structure. The detailed dynamical analysis of residue Cys148 in the linker region of hSTING does not support the earlier hypothesis that Cys148 can form disulfide bonds between adjacent STING dimers. We also reveal that using the full-length proteins is critical as the MD simulations of the LBD portion alone cannot properly describe the global conformational properties of STING.

Introduction

The stimulator of interferon gene (STING) protein has become a focal point in immunological research and future drug discovery for its potential to enhance the ability to fight infection and kill cancerous cells. Recognition of aberrant DNA in the cytosol activates cyclic GMP-AMP synthase (cGAS) to produce a second messenger ligand, cGAMP, which binds and activates STING[1]. The cGAS-STING pathway triggers multiple signaling cascades leading to the production of Type I interferons (IFNs)[2].

The cGAS-STING signaling pathway can provide protection or resistance against infections; however, improper activation or overactivation may lead to autoinflammation and autoimmune diseases[3]. For instance, STING-associated vasculopathy with onset in infancy (SAVI) leads to perpetual STING activation and inflammation. Aicardi-Goutières syndrome causes mutations in DNA-degrading proteins, leading to the buildup of DNA inside cells, which can inadvertently trigger the activation of STING. These examples suggest that the cGAS-STING pathway plays an integral role in inflammation and autoimmune disease[3]. However, understanding the detailed mechanism of this signaling pathway remains a challenge.

Recently structures of full-length STING proteins, i.e., ligand-unbound open (apo) structure for chicken and human as well as cGAMP ligand-bound closed (holo) structure for chicken, were identified using cryogenic electron microscopy (cryo-EM)[4]. The structures for the apo and holo states are shown in Figure 1(a). In nature, STING exists as a homodimer transmembrane protein, consisting of an N-terminal transmembrane (TM) region, linkers, a C-terminal ligand-binding domain (LBD), and a C-terminal tail (CTT). Additionally, the structure of the ligand-binding site (Figure 1 (b)) displays a V-shaped dimer. In the apo configuration, the CTT is tightly sequestered against the protein's main body for the signaling auto inhibition[5]. The

binding of cGAMP induces an inward rotation of both monomers toward the ligand-binding site with an accompanying four-stranded β-sheet 'lid' that encloses the pocket, shown in Figure 1(c)[4–8].

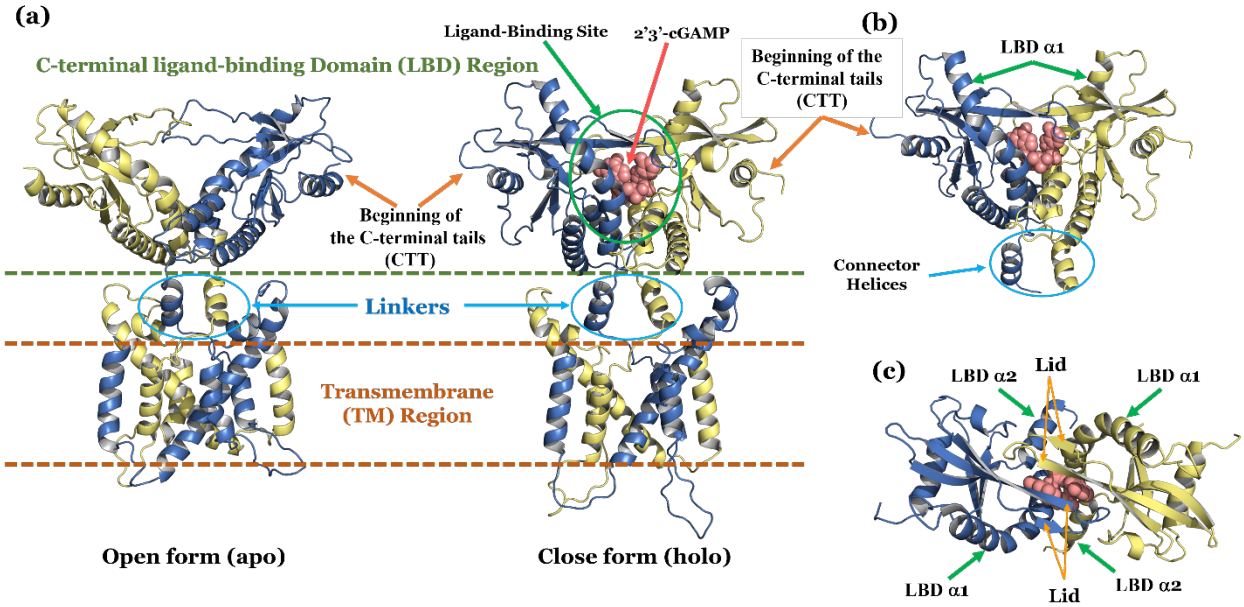

Figure 1 *Structures of full-length hSTING. (a) apo (open) and holo (closed). Apo linker and LBD-α1 portions of the two subunits in the dimer create a right-handed crossover formation. In the holo state, this crossover is no longer formed. (b) The two LBD-α1 helices create the V-shape binding pocket. (c) Top view of STING LBD – β-sheets from chains A and B act as a lid for the binding site.*

The recent cryo-EM experimental result[4] also shows that LBD rotates clockwise relative to the TM domain upon ligand binding (Figure 1(a)). This rotation unwinds the right-handed crossover in the connector helix (as observed in the apo structures) and results in the parallel alignment of the connector helices in Figure 1(b). The study by Ergun et al.[6] showed that the LBD rotational conformation change causes the CTT's to be released, which are otherwise sequestered in the apo structure. This conformational change of CTT's mediates the recruitment of Tank-binding kinase 1 (TBK1)[2,9–12].

Additionally, Shang et al.[4] previously reported that the rotation of the LBD in full-length STING, upon binding cGAMP, is essential. This rotation facilitates the formation of STING

tetramers and higher-order oligomers through side-by-side packing. STING oligomerization allows for TBK1 clustering and trans-autophosphorylation, a process that is not possible without this configuration. Additionally, STING must be phosphorylated to continue the immune signaling response. Ser366, the major phosphorylation site in both human and chicken STING, is located too far away from the active site of TBK1 for STING to be phosphorylated by the same TBK1 to which it is bound[2]. However, in large oligomers, the TBK1 that is tethered to the two CTT's of one STING dimer can phosphorylate the serine residues of CTT's in neighboring STING proteins, which are not bound to this TBK1[2,4].

The phosphorylated residues in the CTT provide a binding site for interferon regulatory factor 3 (IRF3), thereby recruiting IRF3 for phosphorylation via nearby TBK1. Phosphorylated IRF3 forms a dimer that translocates to the nucleus and induces the production of Type I IFNs and other cytokines[2]. Specification of TBK1-mediated IRF3 activation is essential for the tight regulation of IFN production, which would otherwise lead to autoimmune diseases[9].

Even though structural and dynamic effects associated with the biomolecular signaling pathways are complex and not easily recognized through traditional experiments, increasing molecular dynamics (MD) capabilities provide powerful new scientific tools for decoding the signaling pathways. MD simulations facilitate and complement experimental studies by providing detail at the atomic level for molecular interactions in biological systems.

Recently MD simulations were applied to investigate structural and dynamic differences before and after the ligand binding of STING[13–15]. However, all previous studies used only the LBD portion of the protein. Here, we carried out MD simulations for full-length chicken and human STING (chSTING and hSTING) in the membrane environment to explore structural and dynamical differences between them. We show that using the full-length protein is critical as the

MD simulations of the LBD portion alone cannot properly describe the global conformational properties of STING. The global conformational structures are necessary to understand the biological mechanism, including the signaling pathway and the ligand binding process.

chSTING was chosen for this research because the cryo-EM structures for both full-length apo and holo states have been determined and published in the Protein Data Bank (PDB). According to the sequence alignment (supplemental information Figure S1), chSTING shares 44.6% amino acid identity with hSTING. Additionally, the previous experimental study conducted by Shang et al.[4] also confirmed that chSTING and hSTING have very similar apo structures.

Moreover, in general terms, the responses to pathogens are similar in birds and mammals. The two main branches of the immune response (innate and adaptive) and immunological memory generation are present in both classes. However, the mechanisms by which birds and mammals achieve the same overall immune responses are very different[16]. Recent studies have indicated that STING proteins in humans and various animals respond differently to anticancer/antiviral agents and SARS-CoV-2[17]. Consequently, it is valuable to conduct computational studies of chSTING and hSTING in the membrane environment to understand the differences in ligand sensitivities. For these reasons, investigating dynamical differences between chSTING and hSTING is of interest.

Using MD simulations, we answered how STING protein structures in the membrane environment at normal temperature might deviate from the cryo-EM and crystal structures published in the PDB. We looked at ligand-bound closed and ligand-unbound open forms to investigate the conformational and dynamical effects produced via ligand-binding in chSTING

and hSTING. Additionally, we explored the dynamical and structural differences between chSTING and hSTING ligand binding sites.

Furthermore, Ergun and Li's previous study[18] suggested that the uncrossing of the linker region in the hSTING holo-state increases the availability of cysteine residues to form disulfide bonds between neighboring hSTING dimers for polymer stabilization. We investigated the accessibility of cysteine residue 148 (Cys148) located in the linker region of hSTING to explore its possible participation in polymer cross-linking.

Methods

We performed a series of MD simulations of full-length chSTING and hSTING proteins within a membrane environment. Here, we briefly describe our structure modeling and simulation protocols.

Starting Structures: apo-chSTING and apo-hSTING

Previous cryo-EM study[4] has determined both structures for full-length apo-chSTING and apo-hSTING and have been deposited in the PDB. The coordinates for apo-chSTING [PDB ID: 6NT6] and apo-hSTING [PDB ID: 6NT5] were retrieved from the PDB. Since the PDB coordinate structures contained missing residues in the loop and turn regions, MODELLER[18], a protein homology modeling program, was used to resolve this issue. Additionally, since the structures of chSTING and hSTING are very similar to each other[4], the crystal structure of the LBD portion of apo-hSTING [PDB ID: 4F5W] was used as a secondary structural template to refine the LBD portions more accurately using MODELLER[19]. The final model was selected based on the GA341[20] and DOPE[21] scores. GA341 ranges between 0 (worst score) and 1 (best score), while the lowest DOPE value is considered to represent the best model. Even though the

DOPE score has been shown to be an extremely accurate model assessment score in a number of studies[22], a general consensus in comparative protein structure models is to predict absolute accuracy by combining several assessment scores. Since GA341 score is best used for ruling out substandard models, therefore, any models whose values were less than 0.6 were discarded. Then, among the remaining structures, we selected the structure with the lowest DOPE score as our final model. Examples of root-mean-square deviation of the top three assessment score models from the native structure of the apo-hSTING are presented in Figure S2.

Starting Structure: holo-chSTING

The full-length holo-chSTING structure was also previously determined by the cryo-EM study[4]. The structural coordinates [PDB ID: 6NT7] were retrieved from the PDB. Since this coordinate file also had a number of missing residues, we used 6NT7 as the primary MODELLER template to build the initial holo-chSTING structure. The holo-hSTING LBD structure [PDB ID: 4F5D] was also employed as a secondary template to accurately reproduce the holo-chSTING LBD region. Again, the final structure was selected by using the GA341[20] and DOPE[21] scores.

Table 1 PDB Structures used for homology modeling

PDB ID	Descriptions	Experimental Method	Resolution (Å)	Citations
4F5D	human STING LBD with ligand	X-Ray Diffraction	3.00	Shang et al.[23]
4F5W	Ligand free human STING LBD	X-Ray Diffraction	2.20	
6NT5	Full-length human STING in the apo state	Cryo-EM	4.10	Shang et al.[4]
6NT6	Full-length chicken STING in the apo state	Cryo-EM	4.00	
6NT7	Full-length chicken STING in the cGAMP-bound dimeric state	Cryo-EM	4.00	

Starting Structure: holo-hSTING

Unfortunately, the full-length holo-hSTING structure was not yet determined by experimental methods. However, the previously published experiments[4,23] recognized that the structures of apo-chSTING and apo-hSTING are very similar to each other. Therefore, we accepted the assumption that chSTING and hSTING holo-structures would also be very similar. Thus, the full-length holo-chSTING [PDB ID: 6NT7] was used as a primary template for the homology modeling to construct the holo-hSTING model structure via MODELLER[19]. The holo- hSTING LBD structure [PDB ID: 4F5D] was also used as a secondary template to ensure a more accurate model of the LBD region. The final structure was also selected by the GA341[20] and DOPE[21] scores. Table 1 shows a list of PDB structures used to prepare the initial structures for this study.

Simulation Preparations

Once all STING protein models were completely constructed, the CHARMM-GUI web server[24] was applied to build the initial STING membrane complex systems. The lipid bilayer membrane systems had dimensions of 125 × 125 × 25 Å and consisted of 1,2-didecanoyl-sn-glycero-3-phosphocholine (DCPC) lipids. The topology and force-field parameters for the 2'3'-cGAMP molecule were built using CGenFF[25,26].

The MD simulations were performed with the GROMACS 2020 software[27] and the CHARMM36 force field [28]. Each protein/membrane complex was initially placed in the center of a 125 × 125 × 155 Å simulation box solvated by TIP3P water molecules[29]. Then, if necessary, potassium or chloride ions were added to neutralize the total system charge.

After assembling the protein/membrane complex, an equilibration was performed to relax the initial system from unrealistic high-energy atom arrangements before MD production

simulations. First, the steepest descent algorithm was used to minimize each system for 5,000 steps. Then, six consecutive equilibrations were performed. Here, we had gradual equilibrations of the initially assembled system; various restraints were applied to the protein, ligand, water, ions, and lipid molecules during these equilibrations, as shown in Table 2. The equilibration processes were similar to those used by Jo et al.[30]

Table 2 *Detailed information on each of six consecutive equilibrations*

	Ensemble[1]	Timesteps (fs)	Equilibration length (ps)	Force constants for Harmonic Restraint[2]			
				Protein Backbone[3]	Protein Sidechain[3]	Lipid[4]	Ligand[3]
1	NVT	1.0	125	4000	2000	1000	4000
2	NVT	1.0	125	2000	1000	400	2000
3	NPT	2.0	125	1000	500	400	1000
4	NPT	2.0	500	500	200	200	500
5	NPT	2.0	500	200	50	40	200
6	NPT	2.0	500	50	0	0	50

[1]NVT – Constant volume and temperature with Berendsen thermostat method[31], and NPT – constant pressure and temperature with Berendsen thermostat and barostat method[31].
[2]Force constants are in kJ/(mol·nm^2)
[3]Positional harmonic restraints
[4]Harmonic restraints for the lipid tail and head group

Production MD Simulations

The last coordinates from the previous gradual equilibration were further processed through a two-step final equilibration. The first step of this final equilibration was to apply a constant number, volume, and temperature (NVT) simulation using the V-rescale algorithm[32] without any position restraints for 200-ps. Another equilibration was conducted at a constant number, pressure, and temperature (NPT) for a 500-ps simulation via the Parrinello-Rahman algorithm[33] at 1 bar pressure and the V-rescale algorithm[32] at 30^{o}C. After these additional equilibrations, multiple production MD simulations were run in the NPT condition.

In all cases, an integration time step of 2.0-fs was used. Periodic boundary conditions were applied in all directions throughout all simulations. The LINCS algorithm[34] was used only to constrain the bonds involving hydrogen atoms. The electrostatic interactions were calculated using a Particle mesh Ewald algorithm[35] with a 12Å cut-off. The trajectories were saved every 50-ps during each simulation for analysis. A model for the holo hSTING MD simulation is presented in Figure S3.

Reproducibility and reliability are essential features of the scientific method, whether experimental or computational. Scientific methods should reproduce the results in a statistical sense regardless of who performs them. However, chaotic dynamical systems, such as MD simulations, are extremely sensitive to initial conditions[36,37]. For instance, in this study, "*replicas*" refers to MD simulations consisting of identical structures, identical parameters, and varying initial velocities randomly assigned via the Maxwell distribution. These replicas often produce different trajectories caused by the roughness of the potential energy surface, which contains many local minima frequently separated by high energy barriers. Thus, the free energy landscape of these simulations is often rugged, and minor differences in the initial conditions can cause replicas to take different paths on the phase-space surface[38]. As a result, we expected to see some differences in dynamical details between the replicas. Thus, conclusions obtained from a single MD simulation are usually insufficient. So, the reproducibility and reliability of MD simulations should be based on an averaged statistical sense.

Since previous STING MD studies[13–15] primarily used two or three replicas of each unique model system to achieve reliable results, we used two replicas for each system, as shown in Table 3. Then, we focused on the underlying similarities between replicas by calculating statistical properties on combined trajectories.

Table 3 *Listing of STING MD Simulations Performed*

Research System	State	Ligand	Number of MD replicas[a]	Simulation Time[b]	Total length
chSTING	apo	None	2	0.75 μs	1.50 μs
chSTING	holo	2'3'-cGAMP	2	0.75 μs	1.50 μs
hSTING	apo	None	2	1.00 μs	2.00 μs
hSTING	holo	2'3'-cGAMP	2	1.00 μs	2.00 μs

[a] This column indicates the number of independent simulations performed for each system. The term "*replicas*" refers to simulations of identical structures with identical parameters where only the initial velocities are created randomly according to a Maxwell distribution.

[b] Length of each independent simulation.

Results & Discussion

We inspected the condition and characteristics of the trajectories using VMD software[39] and then proceeded to analyze the data further. We used our in-house developed Python and R code, GROMACS analysis tools[27], Bio3D[40], and PyMOL[41] to perform the analyses. To remove any potential bias of the initial states, we discarded the first 100-ns MD trajectories. Since homology modeling was used to build the full-length STING proteins, we initially conducted confirmatory analyses to make sure that the computational models we built agreed with the previous experimental[4,7,23,42] and LBD only simulations[13–15]. We analyzed the Cα root mean square deviation (RMSD) and the Cα root mean square fluctuation (RMSF). Each RMSD was calculated with reference to the initial cryo-EM structures of apo-STING (PDB: chSTING: 6NT6, hSTING: 6NT5) and holo-STING (PDB: chSTING: 6NT7, hSTING: MODELLER generated initial structure). Those results are presented in Figures S4-S7. According to these figures, the results for hSTING are within the same range as previously reported findings[4,5]. Additional confirmatory analyses of the LBD structures and the binding site were also conducted. Details of these analyses are explained in the next section. Once our research models

were validated, we conducted further analyses regarding the. LBD rotation and tilting movements, shape characteristics of the STING LBD region, distance between the two monomer chains, and solvent accessibilities of cysteine residues.

Validation analyses for model systems

a. Analysis of Ligand-binding domain (LBD) structures

Previous structural studies[4,6,8] show that both chSTING and hSTING display open LBD conformations in the apo state and that cGAMP binding prompts the LBD to adopt a closed conformation. To confirm these observations quantitatively, we analyzed the angle between the two ligand-binding domain α-helices (LBD-α1) from the two monomer chains. These α-helices consist of residues 160-190 in chSTING and 155-185 in hSTING (Figure S1). However, it was not helpful to use all residues of this helix to define the axis in the angle calculation because during the simulation, the long LBD-α1 helix broke into two separate α-helices. Since the breaking point was around residue 170 in chSTING and residue 165 in hSTING, we used residues 160-170 in chSTING and residues 155-165 in hSTING to define the helix axis for each LBD-α1. Then the angle between these two helix axes was calculated (Figure 2 (a), Table S1).

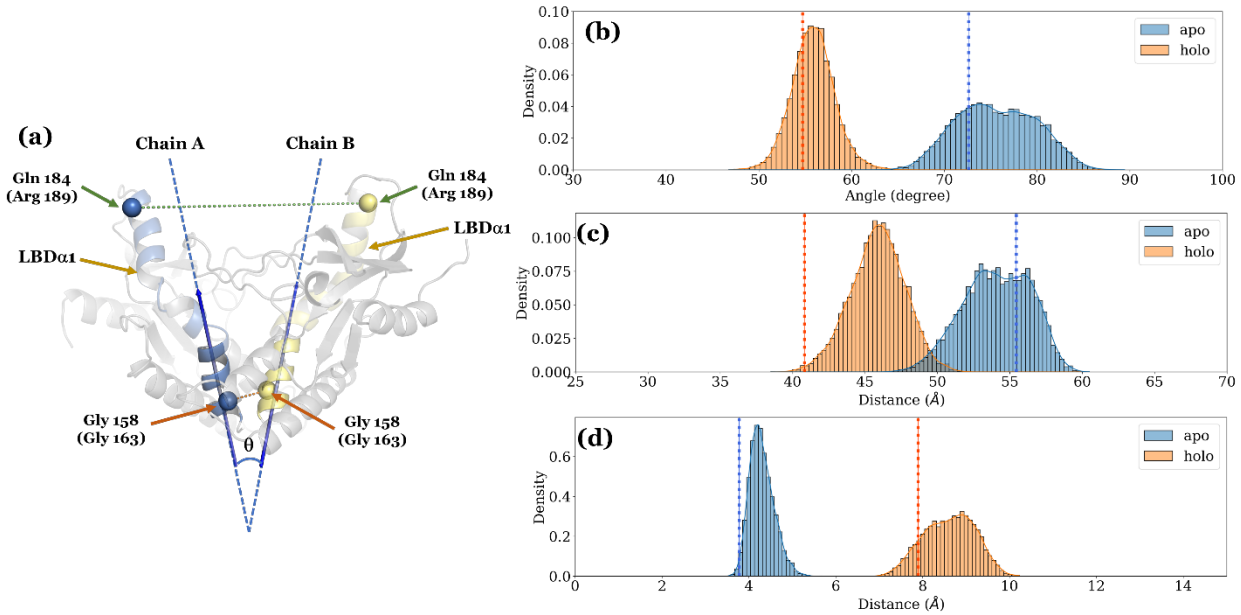

Figure 2 *Geometry of hSTING LBD-α1 helices. (a) The schematic LBD figure shows the definitions of the angle between the two α1-helices, the "tip distance," and the distance between closed-end α1-helices. (b) Distributions of the angles in apo and holo states. (c) and (d) Distributions of distances between Gln184 residues and between Gly158 residues, respectively. Each distribution was calculated with the combined data from two simulations of each system. Vertical lines in (b)-(d) indicate the values from the initial structures – red lines for holo and blue lines for apo.*

The distributions of the angles in apo and holo-structures of hSTING and chSTING simulations are presented in Figure 2(b) and Figure S8(a). There are clear differences in the distributions between the apo and holo-structures: The average angles between LBD-α1 helices in the apo hSTING and chSTING are 75.6 º (± 4.3º) and 70.4º (± 3.1º), respectively. The average angles in the holo hSTING and chSTING are 55.9 º (± 2.3º) and 53.2 º (± 3.2 º), respectively. The angle difference between apo and holo states reinforces the idea that strong intermolecular bonds are formed between cGAMP and LBD, enforcing a more rigid composition and resulting in greater structural stability. These results can be used to classify the basic conformations of the LBD region.

To investigate the open vs. closed conformational change upon ligand binding, we monitored the "*tip distances*" between Gln184 residues in hSTING and between Arg189 residues

in chSTING at the wide-end of the two LBD-α1 helices. According to Figure 2 (b), the "*tip distance*" distributions for apo hSTING and chSTING have peaks at 54.1 Å (± 2.3 Å) and 52.1 Å (± 2.9 Å), respectively. Apo state chSTING (Figure S8 (b)) shows rather large deviations in the distribution compared to hSTING. The average value of apo hSTING agrees with 55.5 Å of the "*tip distance"* measured from the cryo-EM hSTING structure (PDB: 6NT5)[4].

After cGAMP binds, this region closes to produce a tight V-shape conformation with resulting tip distance peaks of 45.9 Å (± 1.9 Å) for hSTING (Figure 2 (c)) and 47.2 Å (± 2.5 Å) for chSTING (Figure S8 (b)). Our simulation observations for the apo and holo states support the experimental observations of the V-shape conformational differences between apo and holo states.

In the apo structures of both hSTING and chSTING, the connector helix and LBD-α1 in the dimer form a right-handed crossover formation that packs closely at one end of the LBD-α1. We measured the distances between conserved glycine residues (hSTING: Gly158; chSTING: Gly163) in the LBD-α1. The average distance between Gly158 in both chains for apo hSTING is 4.3 Å (± 0.3 Å). The average distance between Gly163 residues in apo chSTING is 4.1 Å (± 0.2 Å). According to Figure 2(d), the distribution of the distance between Gly158 in apo hSTING shows relatively small fluctuations throughout the simulations and is similar to the one observed from PDB: 6NT5[4]. However, the chSTING value is slightly larger than the one observed from PDB: 6NT6[4]. Additionally, similar to the "*tip distance*," apo chSTING also displays larger deviations in the Gly163 distance distribution (Figure S8 (c)) than those of hSTING.

In the holo-structure, the direct binding of cGAMP to the middle section of LBD-α1 pushes the two LBD-α1 helices in the dimer away from each other, increasing the average distance between the two glycine residues to 8.6 Å (± 0.6 Å) in human (Figure 2(d)) and 8.4 Å (±

0.6 Å) in chicken STING (Figure S8 (c)). The differences in holo hSTING and chSTING are not significant; a small deviation in the distance is expected due to the natural dynamics of biological systems. The value for chSTING is consistent with the previous experimental result presented by Shang et al.[4]

Previous experiments suggested that the increase in distance between glycine residues from the apo to holo states was caused by the conformational changes induced by cGAMP driving the LBD rotation. The structural observations from our simulations indicate that if the crossover conformation of the connector and the LBD-α1 helices of the two chains, seen in the apo state, was maintained, the outward movement of the LBD -α1 would lead to unnatural bond stretches and nonphysical atom-atom interactions in the connector loop. Thus, our results suggest that increased distance in this region must be followed by conformational changes between apo and holo states. Further analysis to confirm this hypothesis needs to be performed.

b. Analysis for Ligand-Binding Sites

Ligands can affect the protein's stability and conformation. To further describe the dynamical characteristics of STING in the presence of a ligand, we monitored pairwise cross-correlation coefficients, which represent how the atomic fluctuations/displacements of a system are correlated with one another. We investigated the Linear Mutual Information (LMI) maps[43] of the ligand-binding sites in apo and holo STING. Despite its widespread usage, dynamical cross-correlation (DCC) maps have weaknesses. If two atoms move in perpendicular directions simultaneously, their correlation cannot be measured with DCC due to the dot product involved in its calculation. Instead, LMI is a parameter that has no unwanted dependency on the relative orientation of the fluctuations as encountered in DCC[44]. LMI maps of individual replicas for

hSTING with moderate to strong correlations are shown in Figures S9. As mentioned previously, replicas with different initial velocities are expected to exhibit some differences. Focusing on the underlying similarities between replicas, we present the averaged LMI maps for hSTING in Figure 3 and chSTING in Figure S10. The apo state shows significant correlations between chains A and B (Figures 3 (a) and S10 (a)); however, the holo state (Figure 3 (b) and Figure S10 (b)) displays notably less correlations between chains. These observations suggest that the ligand heavily regulates the dynamics of the ligand-binding domain in holo STING structures. Our observations also indicate that ligand binding enforces a more rigid composition in the LBD.

Additionally, the LMI maps for both chSTING and hSTING, as shown in Figures 3, S9, and S10, exhibit asymmetry in the monomer chain dynamics. These observations indicate the differences in self-correlation between chains A and B despite their homodimer nature.

To get better insight into how the ligand binds to STING and influences its dynamics, we identified the residues that come in contact with the ligand. Here, if any atoms of the residues, except hydrogens, were within 4.0 Å of the cGAMP atoms, we considered those to be contact residues. Additionally, a hydrogen bond (h-bond) was considered to be formed when the donor (D) – acceptor (A) distance was within 3.5 Å, and the D-H-A angle was less than 45^{o}. We expected to see high on and off rates of both contact residues and h-bonds in our analyses. For example, angle changes of a few degrees between the donor and acceptor can influence the presence/absence of an h-bond. In order to eliminate both weaker h-bonds and residue contacts as well as emphasize the important and consistent interactions throughout the simulations, the averaged density distributions of the two replicas for hSTING and chSTING are shown in Figures 3(c) and S11, respectively.

Figure 3(c) characterizes the frequencies of h-bonds between residues in cGAMP-bound hSTING during the MD simulations. There are consistent and stable h-bonds between Thr263 in hSTING (chSTING: Ser268) and cGAMP. Arg238, located in the β-sheet lid, occasionally forms h-bonds with cGAMP. However, based on this analysis, h-bonds from the β-sheet "lids" are not consistent interactions. The numbers of stable h-bonds between the ligand and protein are shown in Figure 3(c).

Our other study[45] showed that the binding free energy of cGAMP in hSTING was -34.8 ± 2.0 kcal/mol, which indicates stable and strong binding. A recent publication by Chen et al.[15] reported that the total binding-free energy between STING and cGAMP is -53.1 kcal/mol. The differences between these two binding energy values may originate from the different free-energy calculation methods (Slow growth[46] used in our study vs. molecular mechanics Poisson–Boltzmann surface area[47] used by Chen et al.[15]) and force field parameters (CHARMM 36[28] in our study vs. AMBER99SB-ildn[48] used by Chen et al.[15]) used in the studies. However, our structural observations in the LBD agreed with those reported by Chen et al.[15]. Both simulation studies conclude that hydrogen bonds do not provide enough binding energy to explain the stability found within the ligand-binding site. Other intermolecular interactions are necessary to stabilize the ligand in the binding site.

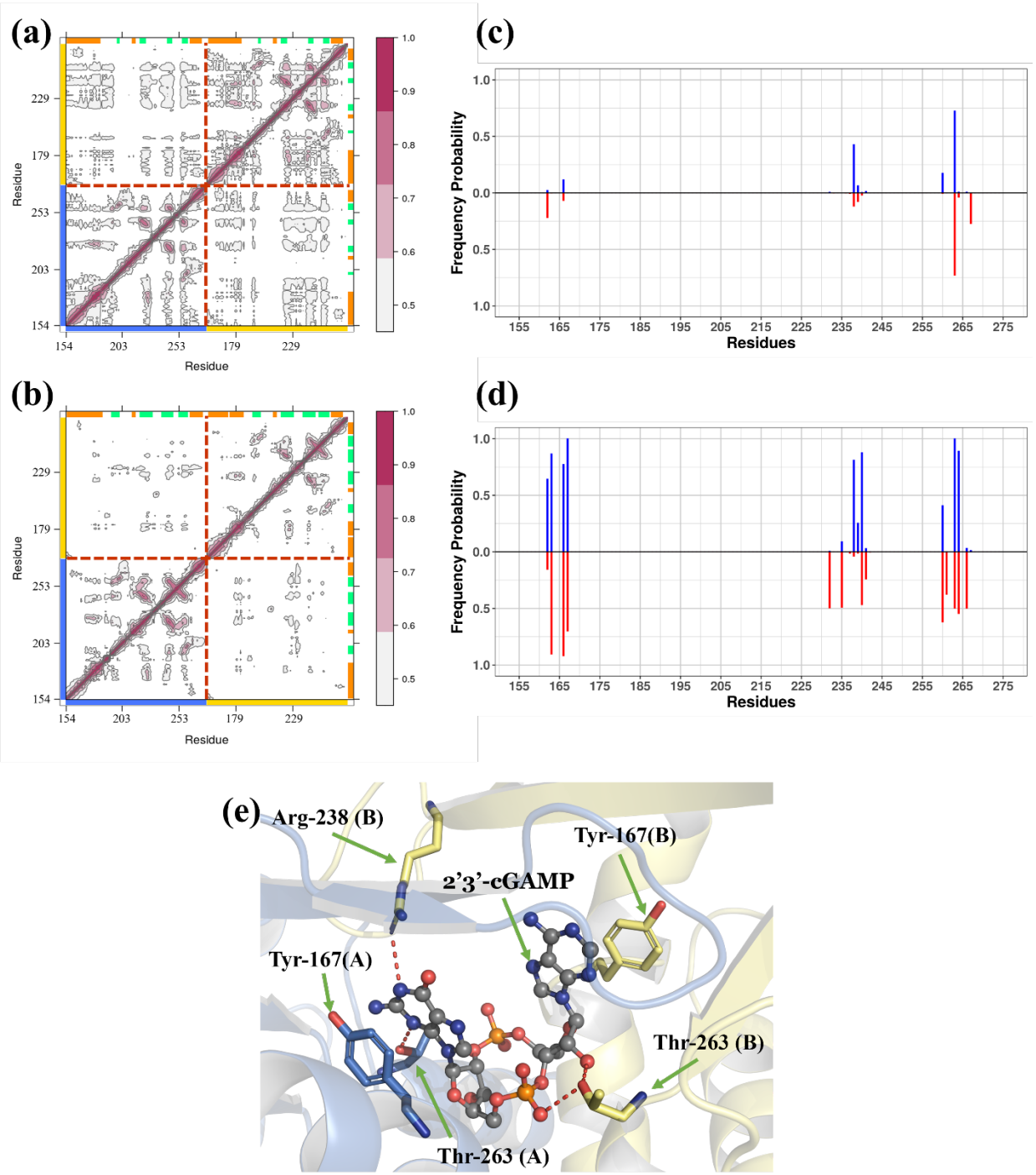

Figure 3 *Averaged Linear Mutual Information maps between residues 154 and 277 of chains A and B. (a) apo hSTING (b) holo hSTING. The blue and yellow axes indicate residues in chains A and B, respectively. Secondary structures are presented by orange blocks (α-helices) and green blocks (β-sheets). All correlations in the holo state are significantly weaker than those of the apo state. (c) Averaged histogram for hydrogen bonding between ligand and residues in hSTING – blue and red indicate residues in chains A and B, respectively. (d) Closed contact histogram: the probability of residues within 4.0 Å of ligand during the simulation – blue and red indicate residues in chains A and B, respectively. (e) Snapshot (at 200-ns) of the ligand binding to STING. The red dotted lines indicate hydrogen bonds.*

According to Figure 3 (d), hSTING has a fair number of residues in contact with cGAMP. This demonstrates that conserved residues between chSTING and hSTING, such as Ser162, Tyr163, Gly166, Tyr167, Arg232, Arg238, Tyr230, and Pro264 (in hSTING, the sequence shown in Figure S1) play significant roles in protein-ligand contact; forming van der Waals and Coulomb interactions with cGAMP. Additionally, in hSTING, a few non-conserved residues, such as Ser241 and Thr263 are also involved in cGAMP interactions.

Figure 3 (e) displays important intermolecular interactions between hSTING and cGAMP, specifically, the close contacts between the ligand and Tyr167 residues in chains A and B. The close contact of Tyr167 elucidates the π–π stacking patterns of the benzene-like ring of the ligand and the aromatic residue of hSTING. In other words, cGAMP is held between these two tyrosine residues by the π–π stacking interaction. These interactions combined with h-bonds, van der Waals, and electrostatic interactions provide enough stabilizing forces to keep the cGAMP ligand in the binding site. Very similar π–π stacking interactions by Tyr172 in chSTING were also observed.

The study by Chen et al.[15] also reported the importance of π–π stacking interactions for stabilization in the ligand in the binding site. Additionally, they reported each residue's contribution to the binding free energies[15]. In our future study, we will expand our analysis to investigate the details of the binding free energy.

Full-length STING structural analyses

The validation analyses confirm that our full-length STING models agree with the previously established LBD portion dynamics and structural behavior of STING. Next, we

present original full-length structural studies that investigate the global conformational properties of STING.

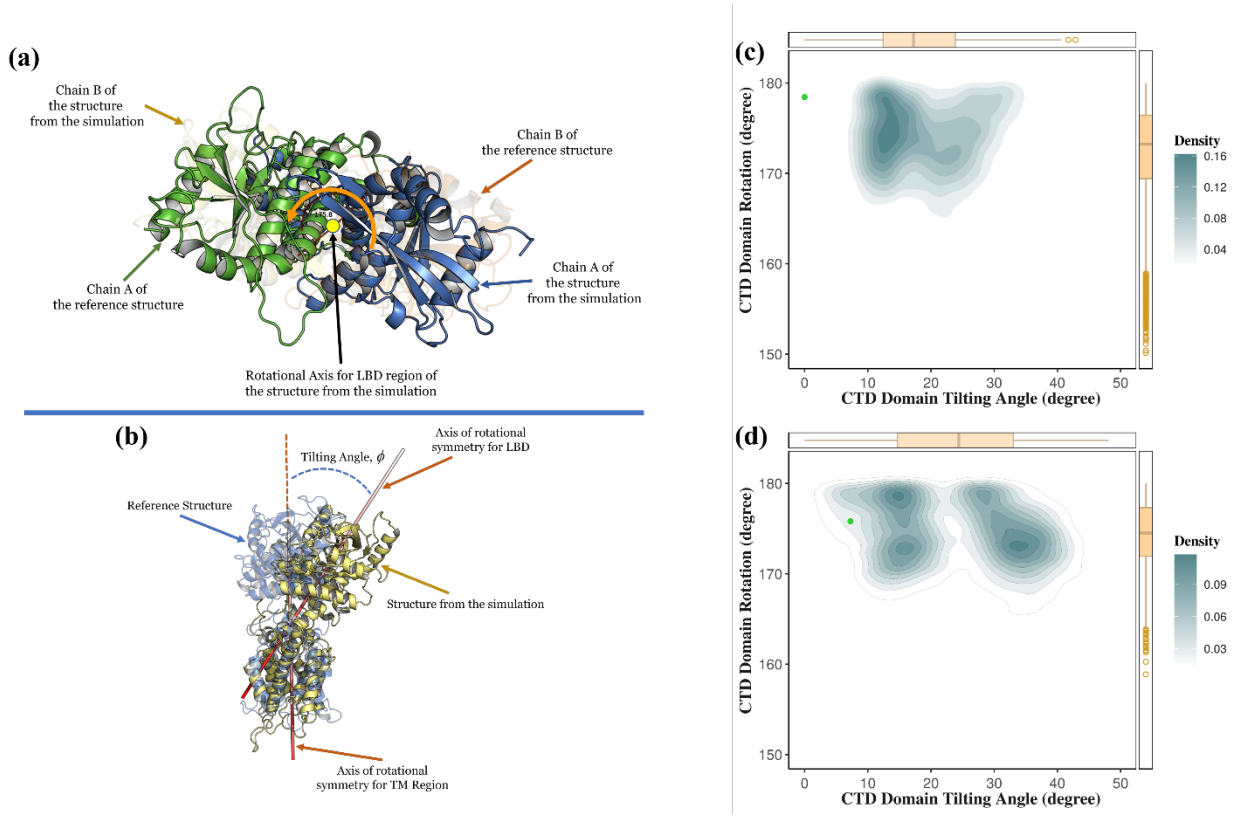

Figure 4 *Rotational and Tilting Dynamics of STING from last 500-ns simulation trajectories. (a) The rotational angle of the LBD with respect to the initial cryo-EM apo structure. (b) Tilting angle is defined as the angle between two axes of rotational symmetry – one for the LBD and another for the TM region. (c) and (d) 2-D histogram of chSTING and hSTING LBD tilting and rotational angle. In (c), the green dot indicates angle values from apo and holo chSTING cryo-EM structures (PDB: 6NT6 and 6NT7). In (d), the green dot indicates angle values from apo (PDB 6NT5) and homologically modeled initial holo hSTING structure. Note: the box-and-whisker plots on the sides of the 2-D histogram describe the distributions of tilting and LBD rotational angles. Each graph was generated with the combined data from two simulations of each system.*

a. Analysis for Ligand-Binding Domain (LBD) rotation and tilting movements

Since segmental flexibility is likely a dominant feature of numerous proteins composed of multiple connected domains, we were interested in understanding the flexibility between the LBD and TM regions present in the membrane environment. Therefore, we examined the rotation and tilting movements of STING with respect to the reference structures. The cryo-EM apo state model (chSTING:6NT6, hSTING: 6NT5) was set as the reference structure. First, the

TM regions of both reference and simulated structures were aligned by performing a sequence alignment followed by a structural superposition. Then, because STING is a homodimer, the axes of rotational symmetry for the TM and LBD regions were separately evaluated for both the reference and simulated structures.

The rotational angle of the LBD (Figure 4(a), Table S2) was extracted from the transformation matrix between the LBD of the reference and simulated structures. The tilting angle of the LBD region with respect to the TM region was defined as the angle between two axes of rotational symmetry – one for the LBD and another for the TM regions (Figure 4 (b)). Results for holo chSTING and hSTING are presented in Figures 4(c) and (d). (The apo results are shown in Figure S12.)

Our results showed that holo chSTING had an average LBD rotation relative to the apo structures of 173.8° (± 3.6°). The equivalent rotation for hSTING was 174.4° (± 3.5°). These results differ from the 180° rotation observed in the cryo-EM experiment[4]. The difference between our observations and reported findings[4] could be a result of cryogenic vs. membrane environment research systems. However, future experimental testing would aid in confirming the reasoning for this difference.

In addition, according to Figures S13 (a) and (b), the average LBD rotations from the initial cryo-EM structures are 34.1° (± 7.7°) and 15.8° (± 7.5°) for apo chSTING and hSTING, respectively. These observations suggest that there are large deviations from the cryo-EM structures and that STING proteins are flexible in the membrane environment.

Investigation into STING's tilting dynamics is unique to our work. Excluding the research conducted by Shang et al.[4], all previous simulation and experimental research studies have only used the LBD structures. Additionally, there are no previous studies that have included

the membrane system in their research model. Therefore, this is an initial investigation into full-length STING dynamics with the inclusion of a membrane system. Since the LBD region is located in the cytosol of the cell, the movement of the LBD with respect to the membrane surface is important to understand the flexibility and dynamics of STING in the cytosol.

According to our results, the average tilting angles are 36.1º (± 12.6°) and 11.5º (± 5.3°) for the apo states of chSTING and hSTING, respectively. Apo chSTING has a larger average tilting angle, implying that its LBD tends to lean to one side. However, we do not believe the tilting motion observed has a preferred side.

For the holo states of chSTING and hSTING, we observed 20.7º (± 8.5°) and 23.8º (± 10.4°) tilts. Figures 4 (c) and (d) indicate large fluctuations present in holo chSTING and hSTING. These large fluctuations demonstrate the '*swaying*' nature of the LBD region, resulting from the flexibility of the linker region of the full-length STING in the membrane environment observed in our simulations. As stated previously, STING must be phosphorylated to continue the immune signaling response. Therefore, we believe that the flexibility of the linker region is necessary to facilitate the phosphorylation of hSTING and TBK1 by orienting hSTING's CTT to be in closer proximity to the TBK1 active site. Lack of flexibility or titling capacity would limit the CTT's range and ability to bind TBK1– making this process more difficult and potentially unattainable; however, further investigation is required to confirm.

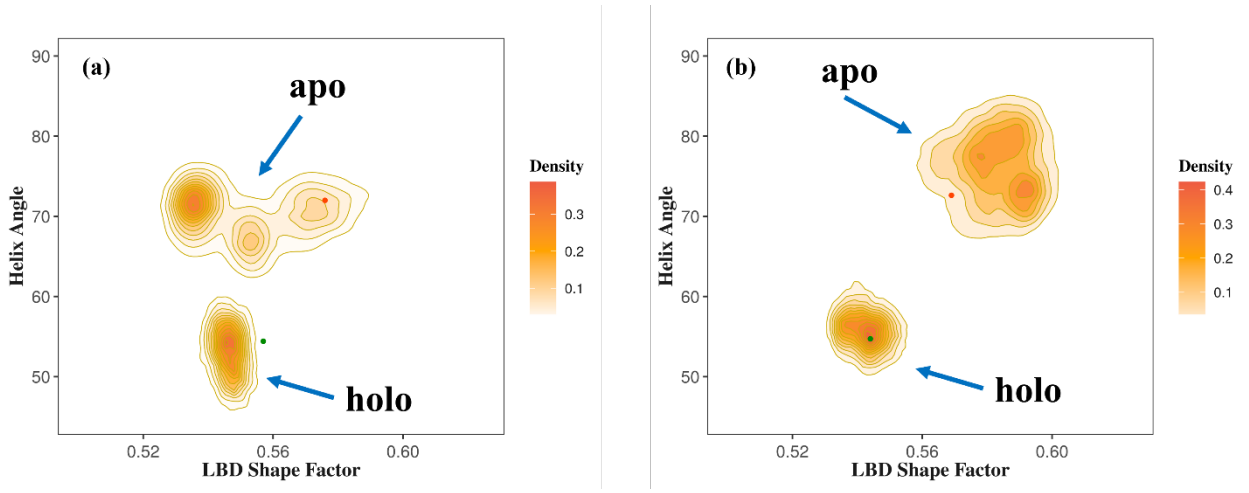

Figure 5 *Density maps for Shape factor vs. angle between two α1-helices, defined in Figure 2. (a) chSTING and (b) hSTING density maps. Each map contains the combined data from two simulations of each system. Green dots indicate the values from initial holo-structures. Red dots show the values from the initial apo structures. For both STING proteins, apo and holo simulations show separated clusters on the maps.*

b. Analysis of the STING LBD shape

To understand how ligand-binding influences the general shape of STING dimers, we evaluated a shape factor, *S*, which describes the relative anisotropic shape of the molecule[49]. The shape factor is defined by three gyration tensors of all LBD Cα coordinates (Human: residues between 150 and 307 and Chicken: residues between 153 and 310 for both chains). The factor ranges from 0 to 1, where $S = 0$ occurs if all Cα atoms in the chain are spherically symmetric and $S = 1$ occurs if all Cα atoms lie on a line. For planar symmetric objects, the relative shape anisotropy converges to the value of 0.25. In Figure S13, we present apo STING structures, which had the minimum and maximum LBD shape factors during the simulations. Although some conformational changes in the LBD can be seen within this shape factor range, the LBD maintains the V-shape conformation. Our results indicate that the apo state of hSTING is slightly more elongated than the holo state. These results support experimental observations that state holo STING adopts a closed conformation whereas apo STING maintains an open conformation. Additionally, apo states for both chSTING and hSTING show much larger fluctuations in shape

factors compared to holo states. This further supports the fact that the ligand interaction stabilizes the LBD region resulting in a more rigid structure.

Apo chSTING in the membrane environment displays a large spread in its shape factor (between 0.52 and 0.6). Additionally, the shape factor decreases to be smaller than those observed in the holo state, despite the wider angles of α1-helices. This indicates that conformational changes occur in the LBD. Snapshots of apo and holo STING structures in the membrane are presented in Figures S14 and S15. The changes in the LBD structures are clearly visible. These results show that the large deviations in shape factors are caused in part by re-organizations of helices in the LBD region. The structural changes in the LBD are also the reason why there are large RMSD deviations present in Figures S4 (a) and S5 (a). Further analysis to explore the reasons for larger structural fluctuations in the apo state of chSTING needs to be performed.

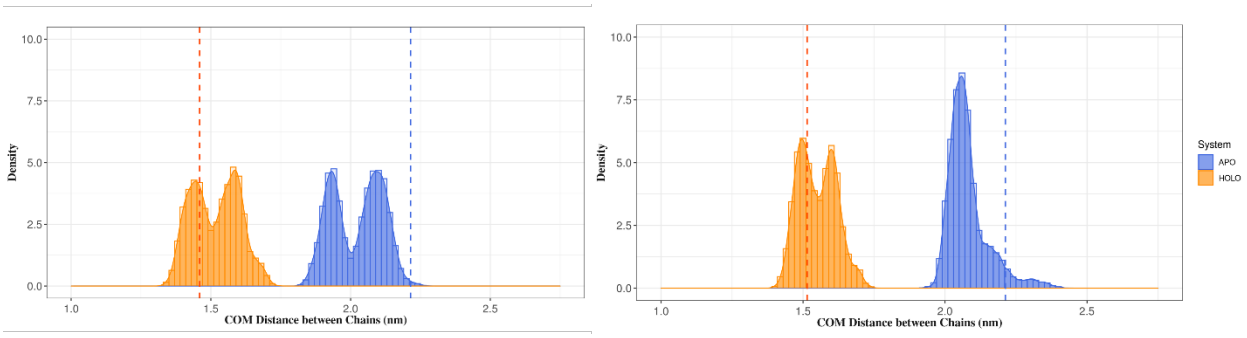

Figure 6 *Distributions of distances between the centers of mass (COM) of two chains during the last 500-ns of simulations: (a) chSTING and (b) hSTING. Each distribution is generated by using the combined data from two simulations of each system. Vertical lines in (a) and (b) indicate the values from the initial structures – red lines for holo and blue lines for apo.*

c. Analysis of the chain's center of mass

Additionally, we measured how the distance between chains A and B's centers of mass (COM) changed during the simulation. Figure 6 presents the results of the COM distributions

from the combined data for the last 500 ns. In the figure, bimodal distributions are the consequences of two independent replicas for each system. However, these differences are very small – which only differ about 1.0 Å. Both chSTING and hSTING's COM distance distribution fluctuated within 2.5 Å from the initial structure. Also, the apo structures of both chSTING and hSTING had smaller COM distances than those of the initial structures.

In summary, we did not observe large shifts in COM values for either chSTING or hSTING, nor did our simulation models display any separation of monomer chains during the production runs. However, this result conflicts with the earlier simulation study by Shih et al.[13], which reported the separation of monomer chains of apo hSTING during their 150-ns implicit solvent simulation. The origin of this conflict should be explored further in future research.

d. Analysis of Cysteine Residues

A previous study by Ergun et al.[6] suggested that Cys148 in hSTING plays an important role in forming inter-dimer disulfide bonds and stabilizing STING tetramers and higher-order oligomers. STING is a homodimer transmembrane protein consisting of TM, linkers, LBD, and CTT regions. The model used by Ergun et al. excluded the TM region of STING (used residues 137-379), which as a result, left the residues located within the connector helices exposed. However, the full-length STING protein in a membrane environment is a more accurate model to test the surface area accessibility of these residues because it mimics how the protein exists naturally in the body. The relative solvent accessibility calculation was used to measure the extent of burial or exposure of that residue in the 3D structure[50]. We calculated the relative per-residue solvent accessible surface area (SASA) of Cys148 using full-length hSTING in the membrane environment to determine if it would be accessible to form disulfide bonds between

neighboring tetramers. Since lipids in the membrane can move upon the formation of an oligomer to expose the cysteine residues, we calculated SASA values by excluding any contributions from the lipids.

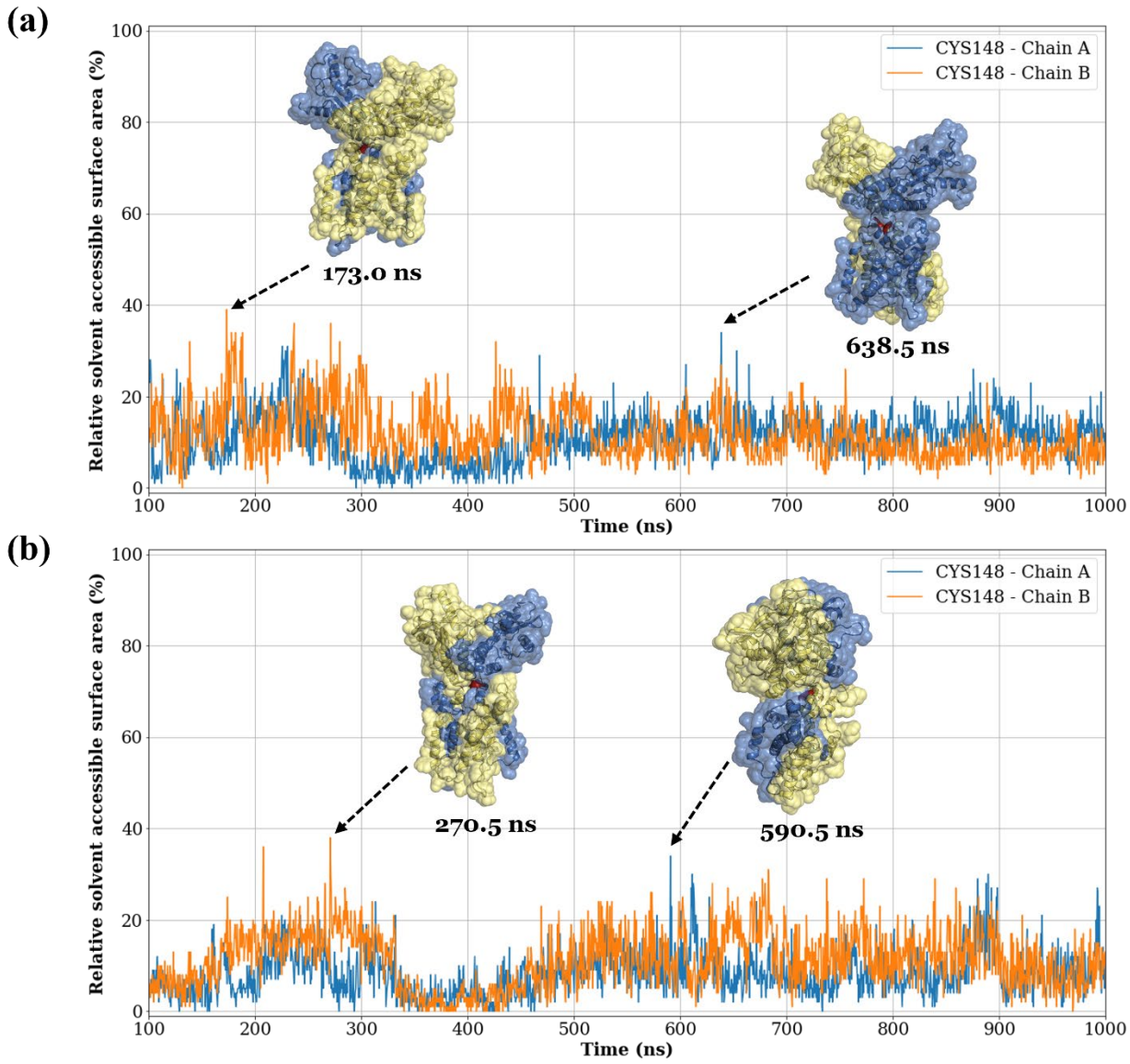

Figure 7 *Comparison of relative solvent accessible surface Areas (SASA) of Cys148 in hSTING. The values vary between 0.0% (fully buried) and 100.0% (fully exposed). Relative SASA of Cys148 in human STING (a) apo state and (b) holo state. Solvent accessible surfaces of selected structures of hSTING during the simulations are shown here. Chain A and B are colored in blue and yellow, respectively. The surface areas of Cys148 are shown in red.*

According to Figures 7 and S16, our results show that residue Cys148 has less than 25% SASA in both apo and holo states. Additionally, our simulations showed that Cys148, located in the linker region, is buried deep within the protein's main body, rendering Cys148 unable to form disulfide bonds between STING tetramers at this location in a membrane environment. As a result, we cannot support the hypothesis that STING forms disulfide bonds via Cys148 because STING occurs naturally as a transmembrane protein and cannot form such bonds under these conditions.

Moreover, cysteine residues are absent from the linker region in chSTING, yet it successfully forms STING tetramers in the holo state[4]. Assuming the cysteine residues in the linker region were required for disulfide bonding between adjacent STING dimers to be activated, then chSTING would not be able to form tetramers or be activated. Therefore, we conclude that Cys148 in hSTING does not contribute to stabilizing the STING tetramer.

On the other hand, Cys281 residues in chSTING, shown in Figures 8 and S18, are located in the LBD loop and are situated in a way that is likely to form disulfide bonds between neighboring STING dimers and could contribute to the formation of STING tetramers. In support of this, the simulation results (Figures 8 and S17) display significant changes in relative SASA between the apo and holo states. Due to the optimal location, large SASA, and lack of other cysteine residues present in the LBD loop that could act similarly, we conclude that Cys281 in chSTING is an ideal candidate for disulfide bonds between adjacent chSTING dimers.

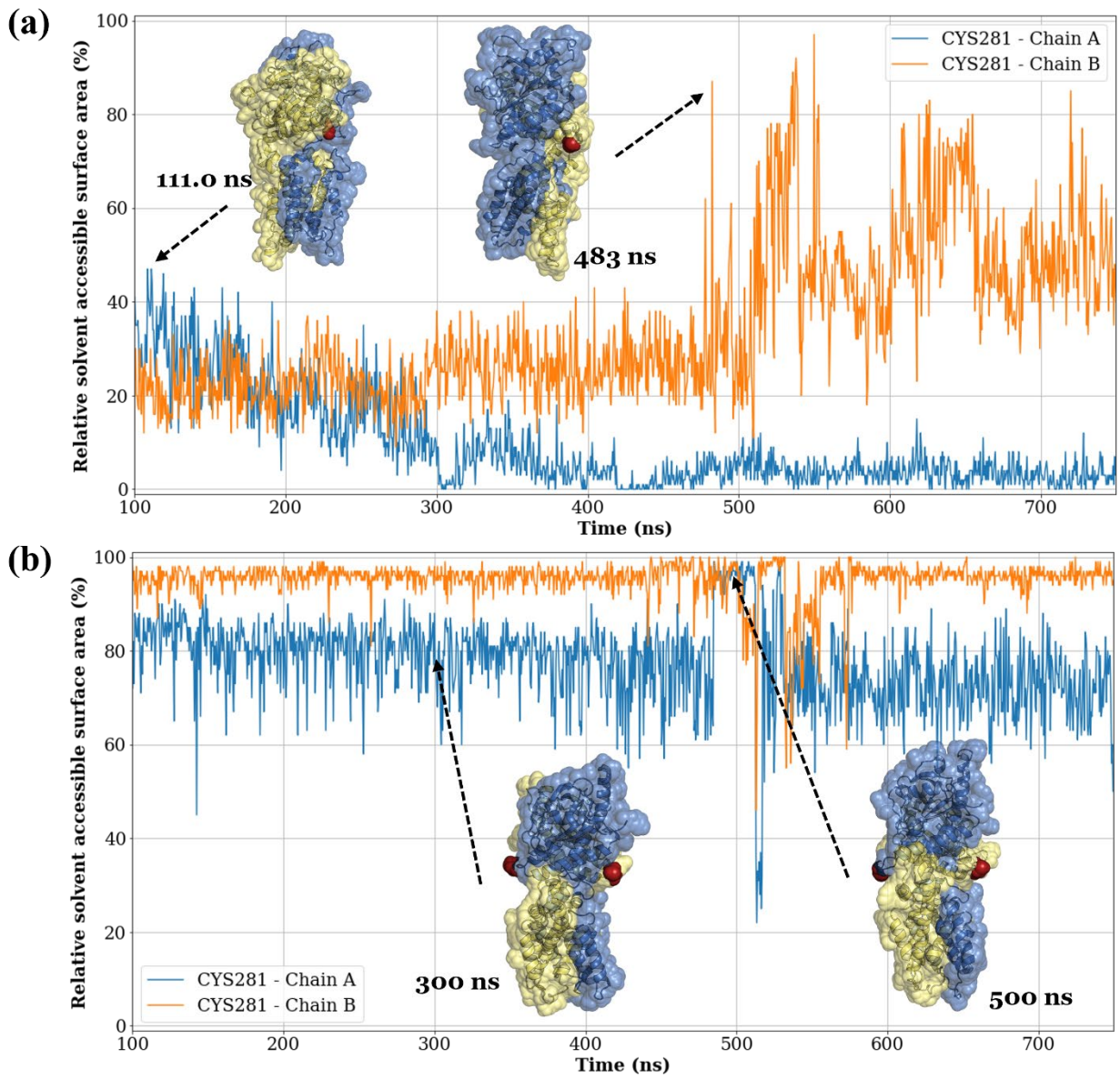

Figure 8 *Comparison of the accessibilities of Cys281 (in red) in chSTING. Cys281 in the apo state (a) is partially exposed, providing only a small portion of available surface area in the STING dimers. However, Cys281 in the holo state (b) is exposed fully, allowing for external interactions. Chain A and B are colored in blue and yellow, respectively. The surface areas of Cys281 are shown in red.*

Since there are no cysteine residues in the vicinity of the LBD loop in hSTING, other cysteine residues besides Cys148 should be further examined to determine if disulfide bonds play a crucial role in the stabilization of STING. The recent study conducted by Ergun et al.[6] suggested that Asp301 of one STING dimer is positioned between Arg281 or Arg284 from a neighboring dimer, allowing for salt bridge formation. The structures obtained from our MD simulations support the idea that the salt bridge could be an essential factor for stabilizing STING tetramers and higher-order oligomers. This hypothesis should be examined in future research.

Conclusion

In summary, using MD simulations, we explored the conformational and dynamical characteristics of full-length apo and holo STING, as well as the interactions between STING and cGAMP within a membrane environment. Our research provides mechanistic insights into the conformation of STING modulated by the cGAMP ligand in a membrane environment. Based on our MD simulation studies, we conclude the following:

First, cGAMP-bound holo STING displays a median value of 174.0° and 174.5° rotation of the LBD relative to the TM region in chSTING and hSTING, respectively. These values differ slightly from the previously proposed 180° [4,18]. The MD simulations showed the LBD swaying back and forth within the cytosol, suggesting that the linker regions of STING are relatively flexible in a membrane environment.

Second, the residues from each chain in the ligand binding pocket are strongly correlated to one another in apo STING compared with those in holo STING. Ligand-binding alters the chain interactions within the LBD, forming a less correlated but more rigid structure.

Furthermore, in our study, monomers in the apo hSTING dimer did not pull apart or exhibit unstable LBD dynamics.

Third, although both chSTING and hSTING display small numbers of steady hydrogen bonds between cGAMP and STING, the binding energy produced is not enough to stabilize the ligand in the binding site. Other intermolecular bonds, such as π–π stacking interactions, are required for stabilization.

Fourth, our analysis of the relative SASA of Cys148 in hSTING reveals that the location of the residues in the linker region would render it impossible to form a disulfide bond with a neighboring STING dimer under the current simulated conditions. Thus, our results do not support the previous hypothesis[6] that Cys148 residues need to form disulfide bonds between adjacent STING dimers to stabilize the STING polymer. Therefore, we have proposed that Cys148 in hSTING does not play a major role in stabilizing STING tetramers.

Some results obtained from our MD simulations and subsequent analyses differ from the findings reported in the previous simulation studies[6,13–15,18]. We attribute these differences to the research model used in those studies, which was composed of only the STING LBD. Since STING occurs naturally as a transmembrane protein, it is imperative that the full-length protein in a membrane system be used to ensure realistic and accurate results.

The information gathered from our MD simulations and subsequent analyses provide an initial look at the structural and dynamical effects induced via cGAMP binding in full-length chicken and human STING in a membrane environment. This research also provides clarification regarding previous studies and proposed hypotheses, increasing our overall understanding of the STING signaling pathway. Our future research will include using computational methods to understand the STING dimer diffusion process in a membrane and how STING forms tetramers.

Data and Software Availability

MODELLER can be obtained from https://salilab.org/modeller. Several open access software from third parties was used: VMD1.9 (http://www.ks.uiuc.edu/Research/vmd), GROMACS (https://www.gromacs.org), and R-based Bio3D (http://thegrantlab.org/bio3d). CHARMM Force Field files are publicly available from http://mackerell.umaryland.edu/charmm_ff.shtml. Molecular structures used are available from https://www.rcsb.org. PyMOL that we used in our research is the commercial version of the software from https://pymol.org. An open-source version of PyMOL is also available to download at https://github.com/schrodinger/pymol-open-source. Also, data and python scripts for our investigation will be provided upon request to the corresponding author.

Supporting Information

Additional information from simulation results as mentioned in the text: Sequence alignment between chSTING and hSTING (Figure S1); Examples of three best candidates for apo-hSTING model (Figure S2); The membrane-protein complex system for our molecular dynamics simulations (Figure S3); Root-mean-square deviations (RMSD) from the initial structures (Figure S4); Ligand Binding Domain (LBD) Root-mean-square deviations (RMSD) from the initial structures (Figure S5); Root-mean-square fluctuation (RMSF) of Cα atoms of chSTING (Figure S6); Root-mean-square fluctuation (RMSF) of Cα of hSTING (Figure S7); Geometry of chSTING LBD α1-helices in the ligand-binding domain (Figure S8); Averaged linear mutual information maps of individual hSTING replicas (Figure S9); Averaged linear mutual information maps of chSTING (Figure S10); Averaged histograms of h-bonds between the

ligand and residues and the close-contact residues for chSTING (Figure S11); 2-D density maps for LBD tilting and rotational angles for apo STING proteins (Figure S12); Examples of LBD structures and their shape factors (Figure S13); Selected snapshots of chSTING with shape factors (Figure S14); Selected snapshots of hSTING with shape factors (Figure S15); Comparison of the accessibilities of Cys148 in hSTING (Figure S16); Comparison of the accessibilities of Cys281 in chSTING (Figure S17); Descriptive statistics of measured values for LBD structures (Table S1); Descriptive statistics of measured values for ligand binding domain rotation and tilting angles (Table S2); Shape factors for different systems (Table S3) (PDF)

Acknowledgment

RTP and MW were funded in part by the Visiting Faculty Program (VFP) and the Science Undergraduate Laboratory Internships (SULI) of the U.S. Department of Energy's (DOE) Office of Science and by the Sustainable Research Pathways (SRP) program, which is a partnership between the Sustainable Horizons Institute and the Lawrence Berkeley National Laboratory. This work was also supported in part by National Institutes of Health (NIH) grants P20 GM103418 and P20 RR016475 from the Kansas Idea Network of Biomedical Research Excellence (K-INBRE) program of the National Institute of General Medical Sciences to MW. The authors also thank the National Energy Research Scientific Computing (NERSC) Center for the allocation of computing hours on the Cori and Perlmutter Supercomputers and, in particular, Dr. Ramana Madupu of DOE for the additional allocation of computing hours.

References

(1) de Oliveira Mann, C. C.; Orzalli, M. H.; King, D. S.; Kagan, J. C.; Lee, A. S. Y.; Kranzusch, P. J. Modular Architecture of the STING C-Terminal Tail Allows Interferon and NF-KB Signaling Adaptation. *Cell Reports* **2019**, *27*, 1165-1175.e5. https://doi.org/10.1016/j.celrep.2019.03.098.

(2) Zhang, C.; Shang, G.; Gui, X.; Zhang, X.; Bai, X.; Chen, Z. J. Structural Basis of STING Binding with and Phosphorylation by TBK1. *Nature* **2019**, *567*, 394–398. https://doi.org/10.1038/s41586-019-1000-2.

(3) Zhou, R.; Xie, X.; Li, X.; Qin, Z.; Wei, C.; Liu, J.; Luo, Y. The Triggers of the CGAS-STING Pathway and the Connection with Inflammatory and Autoimmune Diseases. *Infection, Genetics and Evolution* **2020**, *77*, 104094. https://doi.org/10.1016/j.meegid.2019.104094.

(4) Shang, G.; Zhang, C.; Chen, Z. J.; Bai, X.; Zhang, X. Cryo-EM Structures of STING Reveal Its Mechanism of Activation by Cyclic GMP–AMP. *Nature* **2019**, *567*, 389–393. https://doi.org/10.1038/s41586-019-0998-5.

(5) Yin, Q.; Tian, Y.; Kabaleeswaran, V.; Jiang, X.; Tu, D.; Eck, M. J.; Chen, Z. J.; Wu, H. Cyclic Di-GMP Sensing via the Innate Immune Signaling Protein STING. *Molecular Cell* **2012**, *46*, 735–745. https://doi.org/10.1016/j.molcel.2012.05.029.

(6) Ergun, S. L.; Fernandez, D.; Weiss, T. M.; Li, L. STING Polymer Structure Reveals Mechanisms for Activation, Hyperactivation, and Inhibition. *Cell* **2019**, *178*, 290-301.e10. https://doi.org/10.1016/j.cell.2019.05.036.

(7) Zhang, X.; Shi, H.; Wu, J.; Zhang, X.; Sun, L.; Chen, C.; Chen, Z. J. Cyclic GMP-AMP Containing Mixed Phosphodiester Linkages Is An Endogenous High-Affinity Ligand for STING. *Molecular Cell* **2013**, *51*, 226–235. https://doi.org/10.1016/j.molcel.2013.05.022.

(8) Gao, P.; Ascano, M.; Zillinger, T.; Wang, W.; Dai, P.; Serganov, A. A.; Gaffney, B. L.; Shuman, S.; Jones, R. A.; Deng, L.; Hartmann, G.; Barchet, W.; Tuschl, T.; Patel, D. J. Structure-Function Analysis of STING Activation by c[G(2′,5′)PA(3′,5′)p] and Targeting by Antiviral DMXAA. *Cell* **2013**, *154*, 748–762. https://doi.org/10.1016/j.cell.2013.07.023.

(9) Liu, S.; Cai, X.; Wu, J.; Cong, Q.; Chen, X.; Li, T.; Du, F.; Ren, J.; Wu, Y.-T.; Grishin, N. V.; Chen, Z. J. Phosphorylation of Innate Immune Adaptor Proteins MAVS, STING, and TRIF Induces IRF3 Activation. *Science* **2015**, *347*, aaa2630–aaa2630. https://doi.org/10.1126/science.aaa2630.

(10) Wu, J.; Chen, Z. J. Innate Immune Sensing and Signaling of Cytosolic Nucleic Acids. *Annu. Rev. Immunol.* **2014**, *32*, 461–488. https://doi.org/10.1146/annurev-immunol-032713-120156.

(11) Tanaka Yasuo; Chen Zhijian J. STING Specifies IRF3 Phosphorylation by TBK1 in the Cytosolic DNA Signaling Pathway. *Science Signaling* **2012**, *5*, ra20–ra20. https://doi.org/10.1126/scisignal.2002521.

(12) Zhao, B.; Shu, C.; Gao, X.; Sankaran, B.; Du, F.; Shelton, C. L.; Herr, A. B.; Ji, J.-Y.; Li, P. Structural Basis for Concerted Recruitment and Activation of IRF-3 by Innate Immune Adaptor Proteins. *Proc Natl Acad Sci USA* **2016**, *113*, E3403–E3412. https://doi.org/10.1073/pnas.1603269113.

(13) Shih, A. Y.; Damm-Ganamet, K. L.; Mirzadegan, T. Dynamic Structural Differences between Human and Mouse STING Lead to Differing Sensitivity to DMXAA. *Biophysical Journal* **2018**, *114*, 32–39. https://doi.org/10.1016/j.bpj.2017.10.027.

(14) Tehrani, Z. A.; Rulíšek, L.; Černý, J. Molecular Dynamics Simulations Provide Structural Insight into Binding of Cyclic Dinucleotides to Human STING Protein. *Journal of Biomolecular Structure and Dynamics* **2021**, *0*, 1–15. https://doi.org/10.1080/07391102.2021.1942213.
(15) Chen, L.; Zhao, S.; Zhu, Y.; Liu, Y.; Li, H.; Zhao, Q. Molecular Dynamics Simulations Reveal the Modulated Mechanism of STING Conformation. *Interdisciplinary Sciences: Computational Life Sciences* **2021**. https://doi.org/10.1007/s12539-021-00446-3.
(16) Schat, K. A.; Kaspeers, B.; Kaiser, P. *Avian Immunology*, Second edition.; Academic Press: Amsterdam, 2014.
(17) Rui, Y.; Su, J.; Shen, S.; Hu, Y.; Huang, D.; Zheng, W.; Lou, M.; Shi, Y.; Wang, M.; Chen, S.; Zhao, N.; Dong, Q.; Cai, Y.; Xu, R.; Zheng, S.; Yu, X.-F. Unique and Complementary Suppression of CGAS-STING and RNA Sensing- Triggered Innate Immune Responses by SARS-CoV-2 Proteins. *Sig Transduct Target Ther* **2021**, *6*, 123. https://doi.org/10.1038/s41392-021-00515-5.
(18) Ergun, S. L.; Li, L. Structural Insights into STING Signaling. *Trends in Cell Biology* **2020**, *30*, 399–407. https://doi.org/10.1016/j.tcb.2020.01.010.
(19) Webb, B.; Sali, A. Comparative Protein Structure Modeling Using MODELLER. *Current Protocols in Bioinformatics* **2016**, *54*, 5.6.1-5.6.37. https://doi.org/10.1002/cpbi.3.
(20) John, B. Comparative Protein Structure Modeling by Iterative Alignment, Model Building and Model Assessment. *Nucleic Acids Research* **2003**, *31*, 3982–3992. https://doi.org/10.1093/nar/gkg460.
(21) Shen, M.; Sali, A. Statistical Potential for Assessment and Prediction of Protein Structures. *Protein Sci.* **2006**, *15*, 2507–2524. https://doi.org/10.1110/ps.062416606.
(22) Eramian, D.; Eswar, N.; Shen, M.-Y.; Sali, A. How Well Can the Accuracy of Comparative Protein Structure Models Be Predicted? *Protein Sci.* **2008**, *17*, 1881–1893. https://doi.org/10.1110/ps.036061.108.
(23) Shang, G.; Zhu, D.; Li, N.; Zhang, J.; Zhu, C.; Lu, D.; Liu, C.; Yu, Q.; Zhao, Y.; Xu, S.; Gu, L. Crystal Structures of STING Protein Reveal Basis for Recognition of Cyclic Di-GMP. *Nat Struct Mol Biol* **2012**, *19*, 725–727. https://doi.org/10.1038/nsmb.2332.
(24) Lee, J.; Cheng, X.; Swails, J. M.; Yeom, M. S.; Eastman, P. K.; Lemkul, J. A.; Wei, S.; Buckner, J.; Jeong, J. C.; Qi, Y.; Jo, S.; Pande, V. S.; Case, D. A.; Brooks, C. L.; MacKerell, A. D.; Klauda, J. B.; Im, W. CHARMM-GUI Input Generator for NAMD, GROMACS, AMBER, OpenMM, and CHARMM/OpenMM Simulations Using the CHARMM36 Additive Force Field. *J. Chem. Theory Comput.* **2016**, *12*, 405–413. https://doi.org/10.1021/acs.jctc.5b00935.
(25) Vanommeslaeghe, K.; Hatcher, E.; Acharya, C.; Kundu, S.; Zhong, S.; Shim, J.; Darian, E.; Guvench, O.; Lopes, P.; Vorobyov, I.; Mackerell Jr., A. D. CHARMM General Force Field: A Force Field for Drug-like Molecules Compatible with the CHARMM All-Atom Additive Biological Force Fields. *Journal of Computational Chemistry* **2010**, *31*, 671–690. https://doi.org/10.1002/jcc.21367.
(26) Yu, W.; He, X.; Vanommeslaeghe, K.; MacKerell Jr., A. D. Extension of the CHARMM General Force Field to Sulfonyl-Containing Compounds and Its Utility in Biomolecular Simulations. *Journal of Computational Chemistry* **2012**, *33*, 2451–2468. https://doi.org/10.1002/jcc.23067.
(27) Abraham, M. J.; Murtola, T.; Schulz, R.; Páll, S.; Smith, J. C.; Hess, B.; Lindahl, E. GROMACS: High Performance Molecular Simulations through Multi-Level Parallelism

from Laptops to Supercomputers. *SoftwareX* **2015**, *1–2*, 19–25. https://doi.org/10.1016/j.softx.2015.06.001.
(28) Huang, J.; MacKerell Jr, A. D. CHARMM36 All-Atom Additive Protein Force Field: Validation Based on Comparison to NMR Data. *Journal of Computational Chemistry* **2013**, *34*, 2135–2145. https://doi.org/10.1002/jcc.23354.
(29) Mark, P.; Nilsson, L. Structure and Dynamics of the TIP3P, SPC, and SPC/E Water Models at 298 K. *J. Phys. Chem. A* **2001**, *105*, 9954–9960. https://doi.org/10.1021/jp003020w.
(30) Jo, S.; Kim, T.; Im, W. Automated Builder and Database of Protein/Membrane Complexes for Molecular Dynamics Simulations. *PLoS ONE* **2007**, *2*, e880. https://doi.org/10.1371/journal.pone.0000880.
(31) Berendsen, H. J. C.; Postma, J. P. M.; van Gunsteren, W. F.; DiNola, A.; Haak, J. R. Molecular Dynamics with Coupling to an External Bath. *J. Chem. Phys.* **1984**, *81*, 3684–3690. https://doi.org/10.1063/1.448118.
(32) Bussi, G.; Donadio, D.; Parrinello, M. Canonical Sampling through Velocity Rescaling. *J. Chem. Phys.* **2007**, *126*, 014101. https://doi.org/10.1063/1.2408420.
(33) Parrinello, M.; Rahman, A. Polymorphic Transitions in Single Crystals: A New Molecular Dynamics Method. *Journal of Applied Physics* **1981**, *52*, 7182–7190. https://doi.org/10.1063/1.328693.
(34) Hess, B.; Bekker, H.; Berendsen, H. J. C.; Fraaije, J. G. E. M. LINCS: A Linear Constraint Solver for Molecular Simulations. *Journal of Computational Chemistry* **1997**, *18*, 1463–1472. https://doi.org/10.1002/(SICI)1096-987X(199709)18:12<1463::AID-JCC4>3.0.CO;2-H.
(35) Essmann, U.; Perera, L.; Berkowitz, M. L.; Darden, T.; Lee, H.; Pedersen, L. G. A Smooth Particle Mesh Ewald Method. *J. Chem. Phys.* **1995**, *103*, 8577–8593. https://doi.org/10.1063/1.470117.
(36) Knapp, B.; Ospina, L.; Deane, C. M. Avoiding False Positive Conclusions in Molecular Simulation: The Importance of Replicas. *J. Chem. Theory Comput.* **2018**, *14*, 6127–6138. https://doi.org/10.1021/acs.jctc.8b00391.
(37) Wan, S.; Sinclair, R. C.; Coveney, P. V. Uncertainty Quantification in Classical Molecular Dynamics. *Phil. Trans. R. Soc. A.* **2021**, *379*, rsta.2020.0082, 20200082. https://doi.org/10.1098/rsta.2020.0082.
(38) Chong, S.-H.; Im, H.; Ham, S. Explicit Characterization of the Free Energy Landscape of PKID–KIX Coupled Folding and Binding. *ACS Cent. Sci.* **2019**, *5*, 1342–1351. https://doi.org/10.1021/acscentsci.9b00200.
(39) Humphrey, W.; Dalke, A.; Schulten, K. VMD – Visual Molecular Dynamics. *Journal of Molecular Graphics* **1996**, *14*, 33–38.
(40) Grant, B. J.; Skjærven, L.; Yao, X. The Bio3D Packages for Structural Bioinformatics. *Protein Science* **2021**, *30*, 20–30. https://doi.org/10.1002/pro.3923.
(41) Schrödinger, LLC. The PyMOL Molecular Graphics System, Version 2.5, 2015.
(42) Huang, Y.-H.; Liu, X.-Y.; Du, X.-X.; Jiang, Z.-F.; Su, X.-D. The Structural Basis for the Sensing and Binding of Cyclic Di-GMP by STING. *Nat Struct Mol Biol* **2012**, *19*, 728–730. https://doi.org/10.1038/nsmb.2333.
(43) Lange, O. F.; Grubmüller, H. Generalized Correlation for Biomolecular Dynamics. *Proteins: Structure, Function, and Bioinformatics* **2006**, *62*, 1053–1061. https://doi.org/10.1002/prot.20784.

(44) Tekpinar, M.; Neron, B.; Delarue, M. Extracting Dynamical Correlations and Identifying Key Residues for Allosteric Communication in Proteins by *Correlationplus*. *J. Chem. Inf. Model.* **2021**, *61*, 4832–4838. https://doi.org/10.1021/acs.jcim.1c00742.
(45) Payne, R.; Crivelli, S.; Pfeifer, H.; Le, L.; Watanabe, M. Computational Study of Structural and Energetic Effects on Human STING Protein by CGAMP and DMXAA Ligands. *Manuscript in preparation.*
(46) Hu, H.; Yun, R. H.; Hermans, J. Reversibility of Free Energy Simulations: Slow Growth May Have a Unique Advantage. (With a Note on Use of Ewald Summation). *Molecular Simulation* **2002**, *28*, 67–80. https://doi.org/10.1080/08927020211971.
(47) Gouda, H.; Kuntz, I. D.; Case, D. A.; Kollman, P. A. Free Energy Calculations for Theophylline Binding to an RNA Aptamer: Comparison of MM-PBSA and Thermodynamic Integration Methods. *Biopolymers* **2003**, *68*, 16–34. https://doi.org/10.1002/bip.10270.
(48) Hornak, V.; Abel, R.; Okur, A.; Strockbine, B.; Roitberg, A.; Simmerling, C. Comparison of Multiple Amber Force Fields and Development of Improved Protein Backbone Parameters. *Proteins: Structure, Function, and Bioinformatics* **2006**, *65*, 712–725. https://doi.org/10.1002/prot.21123.
(49) Theodorou, D. N.; Suter, U. W. Shape of Unperturbed Linear Polymers: Polypropylene. *Macromolecules* **1985**, *18*, 1206–1214. https://doi.org/10.1021/ma00148a028.
(50) Tien, M. Z.; Meyer, A. G.; Sydykova, D. K.; Spielman, S. J.; Wilke, C. O. Maximum Allowed Solvent Accessibilites of Residues in Proteins. *PLoS ONE* **2013**, *8*, e80635. https://doi.org/10.1371/journal.pone.0080635.